Stony Brook University

Effects of polymer adsorbed layers on the formation of perpendicular cylindrical microdomains in polystyrene-block-poly (ethylene butylene) block- polystyrene (SEBS) ultrathin films

A Thesis Presented

by

Xiaoyu Di

to

The Graduate School

in Partial Fulfillment of the

Requirements

for the Degree of

Master of Science

in

Materials Science and Engineering

Stony Brook University

August 2014

Stony Brook University

The Graduate School

Xiaoyu Di

We, the thesis committee for the above candidate for the
Master of Science degree, hereby recommend
acceptance of this thesis.

Tadanori Koga – Thesis Advisor
Associate Professor, Department of Materials Science and Engineering

Jonathon Sokolov– Second Reader
Professor, Department of Materials Science and Engineering

T. A. Venkatesh – Third Reader
Associate Professor, Department of Materials Science and Engineering

This thesis is accepted by the Graduate School

Charles Taber

Dean of the Graduate School

Effects of polymer adsorbed layers on the formation of perpendicular cylindrical microdomains in polystyrene-block-poly (ethylene butylene) block- polystyrene (SEBS) ultrathin films

by

Xiaoyu Di

Master of Science

in

Materials Science and Engineering

Stony Brook University

2014

Abstract

Block copolymers (BCP) thin films have recently received significant attentions because of their potential "nano" applications, such as nanostructured membranes, nanoparticle templates, photovoltaic cells, low-*k* dielectrics, and high density data storage media. In this study, I focus on perpendicular cylindrical microdomain structures formed in polystyrene -block-poly (ethylene butylene) block- polystyrene (SEBS) block copolymer ultrathin films (less than 100 nm thick). After prolong high temperature annealing of spin-cast SEBS ultrathin films prepared on silicon substrates, a combined use of atomic force microscopy (AFM) and grazing incident small angle X-ray scattering (GISAXS) experiments proved the formation of highly ordered perpendicular cylindrical microdomain structures within the entire films. However, it was also found that the polymer chains strongly adsorbed on the substrates even after intensive solvent leaching with a good solvent for the polymers, resulting in the formation of irreversibly adsorbed polymer layers. A series of x-ray reflectivity measurements revealed that the thickness of the adsorbed layer increases with increasing annealing time before reaching the "quasiequilibrium" thickness (~ 10 nm in thickness after 123 h). The detailed structures of the adsorbed layers were further characterized by AFM and GISAXS, clarifying the formation process of the adsorbed layer. In

addition, I have successfully prepared a variety of adsorbed layers composed of SEBS, polystyrene and polybutadiene homopolymers and studied the possibility to use them an alternative polymer coating materials in place of end-grafted polymer brushes. The experimental results clearly show that the morphologies of the SEBS ultrathin films on top of the adsorbed layer vary with a choice of the adsorbed layer: the PS adsorbed layer is the best to create well-ordered perpendicular cylindrical microdomain structures, while the SEBS adsorbed layer induces parallel cylindrical microdomain orientation instead. Hence, the present study proposes a new way to manipulate the orientation and degree of ordering of microdomain structures in BCP ultrathin films.

Table of Contents

List of Figures

List of schemes

List of Abbreviations

BCP: Block Copolymers

SEBS: Poly (styrene-block-ethylene-butadiene-block-styrene)

PS: poly-styrene

PB: Poly-butadiene

AFM: Atomic Force Microscopy

GISAXS: Grazing Incident Small Angle X-ray Scattering

Acknowledgments

Firstly, I would like to express my deepest appreciation to my thesis advisor, Tadonori Koga, for his unending mentorship and guidance, helping me to hone and enhance my skills as a master's student. His sagacity as my teacher helped make this research and thesis possible. Throughout my research in the lab, he has imbued me with tremendous knowledge and understanding of polymer science which I will be sure to carry with me in my future endeavors.

My thanks also goes out to Naisheng Jiang, a Ph.D student in Professor Koga's lab, who has supported and helped me copiously during my time as a master's student.

A heartfelt thanks to my parents, Zengmin Han and Ruozhu Di, for their inexorable patience and gracious support of my master's studies as well as their infinite consideration of my wellbeing at Stony Brook University.

Chapter 1 Introduction

1.1 Copolymers at surface and interface

BCP is short for block copolymer, which is a specific kind of copolymer that has two or more homopolymer subunits linked together by covalent bounds. The linear AB diblock is the simplest block copolymer architecture, consisting of a block of type A monomers covalently bonded to a block of type B monomers. By coupling additional A or B blocks to this simple architecture, multiblock copolymers can be obtained. Due to their different chain architectures, block copolymers can be divided into three different groups-diblock copolymers, triblock copolymers, graft block copolymers and random block copolymers[2]. Figure 1 shows different copolymer chain

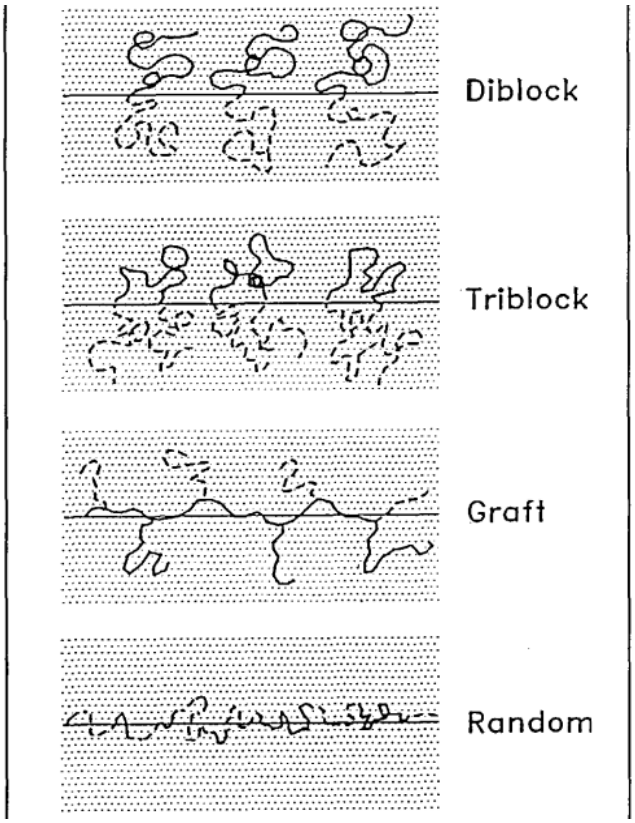

Figure 1. Block copolymer chain architecture at polymer/polymer interface[2].

architectures at polymer/polymer interfaces. Matsen et al[2] did the research on equilibrium behavior of asymmetric ABA triblock copolymer melt and found out that the degree of asymmetry has an effect on the domain spacing and ODTs of block copolymers. As shown in Figure 2, when the

asymmetry becomes sufficiently large, short A blocks begin to pull out of their domains. Although unfavorable interactions occur when an A block leaves its domain, this is more than compensated for by the fact its B block can relax. Figures 2 (a) and 2 (c) demonstrate how the extraction of an

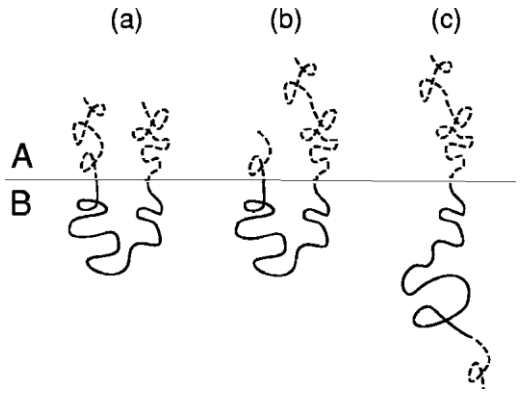

Figure 2. Schematic diagram of three triblock configurations all with equal degrees of chain stretching. Dashed and solid curves denote the A and B blocks, respectively. The symmetric triblock (a) has its segments closest to the interface, while the first asymmetric triblock (b) places its A segments further away and the second asymmetric triblock (c) positions its B segments further away by extracting its short A block from the A domain[1].

A block allows the B segments to shift away from the interface without further stretching of the molecule. Consequently, the continuous extraction of A blocks will reduce the stretching energy of the B domains as t approaches 0. This, in turn, causes a further increase in the domain spacing and shifts the OOTs toward smaller $\boldsymbol{f_A}$.

At polymer/substrate interface, polymer substrate interaction plays very important roll on block copolymer microdomains. T. P. Russel[1] reported that when spin casting PS-b-P2VP on mica substrate, PS block will form micelle microdomains at the surface while P2VP blocks adsorb on the surface due to very strong interaction with the substrate, shown in Figure 3 (a). The sample was annealed for sufficiently long time so that the morphology of micelle structure at free surface is under equilibrium state. Chain conformation of PS-b-P2VP shown in Figure 3 (b) confirm the

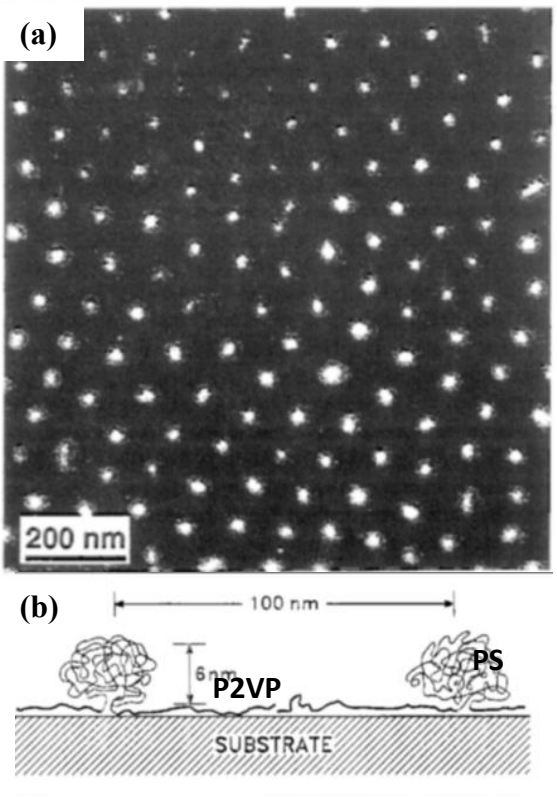

Figure 3. Block copolymer microdomain at polymer/substrate interface. PS microdomains are the bright dot in (a), PS-b-P2VP chain configuration are shown in (b)[1].

1.2 Adsorption kinetics of triblock copolymer at polymer/substrate interface

The adsorption kinetics of block copolymer is more complicated than that of homopolymers. Esskillson[3] studied the adsorption kinetics of triblock copolymer by using time-resolved ellipsometer. His result showed that there are actually three regimes for block copolymer to adsorb, which is different from homopolymer adsorption. Surface coverage here is the main factor during adsorption. As shown in Figure 5, in the first regime where adsorption just started and surface coverage is low, kinetics of copolymer adsorption is diffusion controlled and shows power-law growth with a power around 0.3. In this regime, due to the nature of polymer chain, both of the blocks want to adsorb as many contact as possible on the substrate, resulting in flattened chains on the substrate, as shown in Figure 4 (a). As time increases, surface is covered by more and more polymer chains, adsorption process become slower. In this regime, kinetics is governed by the rate of displacement of anchored weak interaction chains by strong interaction chains. Blocks with weak interaction started to be forced away from the surface and more blocks with strong interaction started to adsorb on the surface, shows in Figure 4 (b) and (c) respectively. At very high surface

coverage regime, the surface is almost saturated. At this time, adsorption process become very slow due to energy barrier caused by the presence of the relatively dense brush of weak interaction

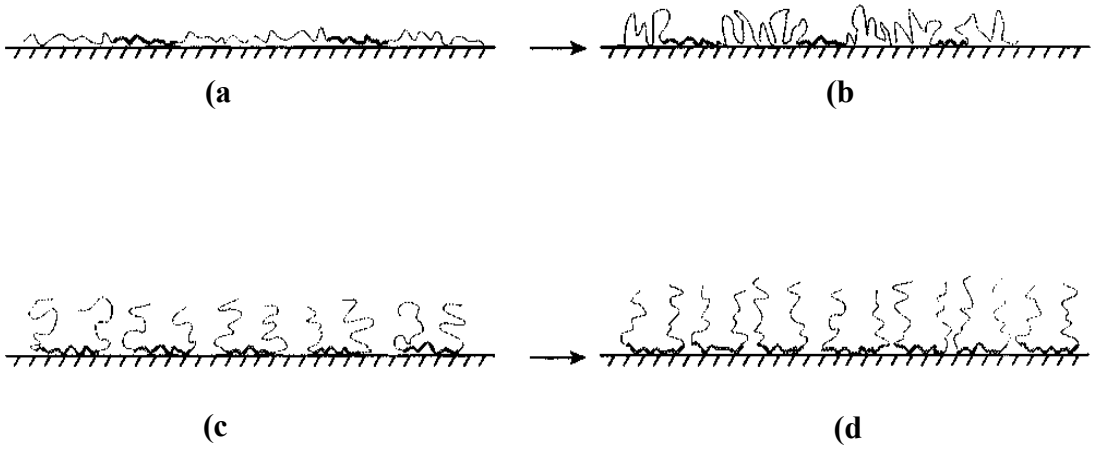

Figure 4. Chain conformation of EO-THF-EO shown in cartoon with different surface coverage. ((a) shows both EO and THF blocks adsorbed on the surface at low surface coverage; (b) and (c) show at intermediate coverage, EO starts to desorb while THF chains take place; (d) shows at very high surface coverage, only THF block adsorb on the surface and form dense EO brush[3].

chains, shows in Figure 4 (d).

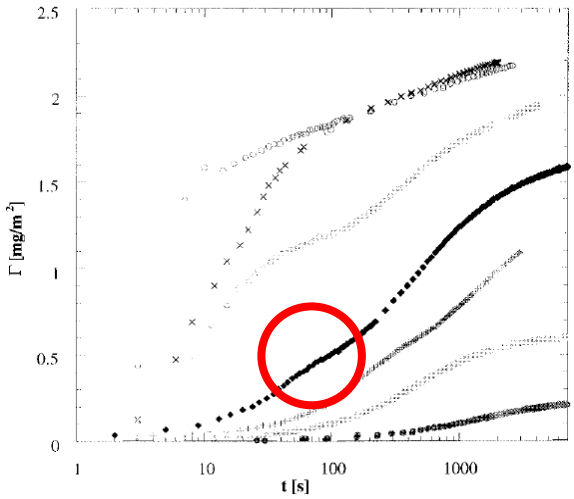

Figure 5. Three regimes in the kinetics of adsorption for EO-THF-EO triblock copolymer. The second regime in red circle is the most essential for block copolymer adsorption[3].

1.3 Effect of adsorbed chains on the nanoconfined block copolymer films

Question raises here is that what effect adsorption has on the microdomain structure of block copolymers. This question has been discussed by many researchers. For example, Harrison[4] and his coworkers reported that PS-b-PB copolymers have different microdomain size when spun cast on different substrate. When PS-b-PB was spun cast on silicon substrate, PB blocks wet the

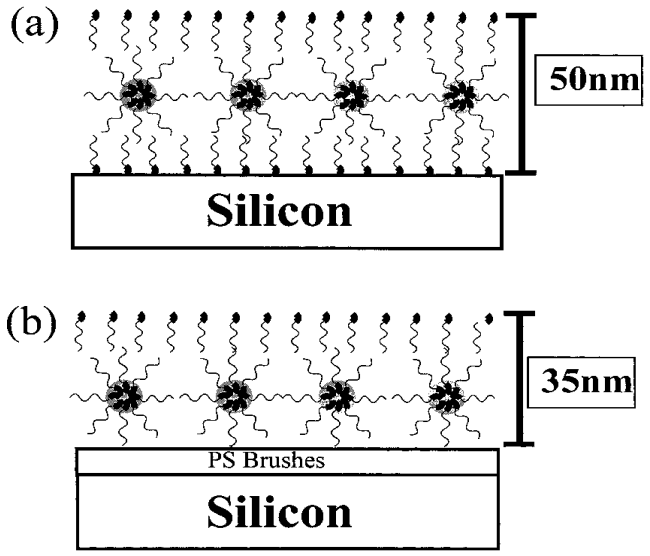

Figure 6. Effect of chain adsorption on copolymer microdomains: (a) on bare silicon; (b) on PS brushes[4].

substrate as it is the lower surface tension component and sandwich microdomain was formed on the substrate, as shown in Figure 6 (a). However, with a layer of PS brush underneath, PB adsorption can be prohibited, as shown in Figure 6 (b).

Effect of polymer/substrate interaction on copolymer microdomains were studied by studying correlation length, shown in Figure 7. They found that SBS polymers are less pinned on the substrate when spun cast on PS brush than on Si, and produce a structure closer to equilibrium state. This phenomenon indicates that when the polymer adsorption effect is reduced or prohibited, polymer can form equilibrium structure faster and more stable.

1.4 Eliminating the Adsorption of Triblock Copolymer Chains on solids with an Irreversible Adsorbed Homopolymer Layer

If the chemically distinct blocks are immiscible, then excess free energy contributions are present

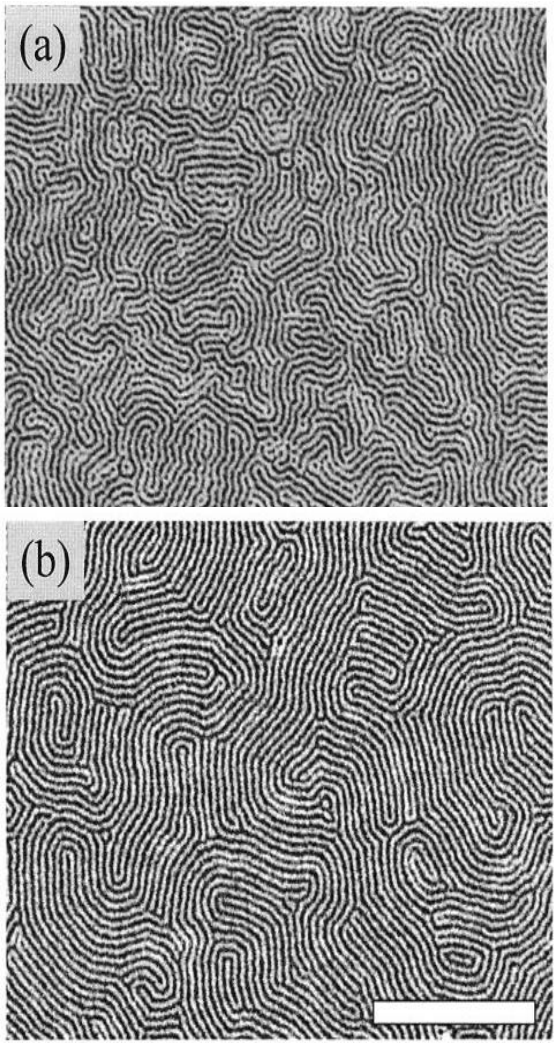

Figure 7. Effect of chain adsorption on copolymer microdomains: (a) on bare silicon; (b) on PS brushes[4].

that discourage mixing. However, in a block copolymer melt, these thermodynamic forces that drive separation are balanced by entropic constraints on the long chain molecules that arise from block connectivity. The morphology of the microphase separated structure depends on three parameters: (1) the Flory chi (ø) parameter between the two monomers, (2) the overall degree of polymerization N, and (3) the composition of the block copolymer f (volume fraction of A segments). Since ø varies inversely with temperature, above the order-disorder transition (ODT) temperature, the block copolymer is a disordered miscible melt. Below the ODT spherical,

cylindrical, lamellar, and the gyroid morphologies with characteristic dimensions of the order of tens of nanometers can be observed.

1.5 Align the block copolymer cylindrical microdomain normal to the surface by eliminating the adsorption between polymer and substrate

At temperature below order-disorder temperature, T_{ODT}, block copolymer can microphases separate into cylinder, lamella, sphere or gyroid microdomains which always exhibits periodic order with repeat distance in the range from 10 nm to 100 nm, depending on the volume fraction of blocks, and the degree of microphase separation, χN, where χ is the Flory-Huggins segmental interaction parameter and N is the total number of segments in block copolymers.[5] The self-assembly of block copolymer into ordered morphology has attract much attention these days for their ability in many applications including drug delivery[6], surface engineering[7] and structure materials. Among these applications, cylindrical nanostructures with microdomains perpendicular to the surface are particularly useful for forming masks for nanolithography[8], templates and scaffolds[9], and membranes[10]. Many works have been done using external force to control the cylindrical microdomain of BCP perpendicular to the surface, including thermal annealing[11], solvent annealing[12,13], electromagnetic fields[14], shear[15], topographically or/and chemically patterned substrates[16]. Among these methods, thermal annealing and solvent annealing are the most widely used since they are simple and straightforward and most importantly, they can be combined with other external force to enhance the perpendicular microdomain orientation of BCP. However, most of the research focus on the surface induced patterning to make cylindrical microdomain normal to the surface. Key to the use of block copolymers for the fabrication of nanostructured materials is controlling the orientation and lateral order of the microdomains in thin films.

Upon knowing the importance of eliminating the adsorption between polymer and substrate, many researches have been done using homopolymer brushes underneath block copolymer thin films to control the microdomain of BCP normal to the surface, along with thermal annealing, solvent annealing, electromagnetic fields, etc. A block copolymer film spin-coated onto such a brush will penetrate into the brush, which promotes adhesion. By fine tuning the composition of

the random copolymer, the interactions of the blocks with the modified substrate can be balanced, and consequently, the microdomains will orient normal to the surface. G. J. Kellogg group use random copolymers of the same components as in a diblock to drive perpendicular orientation of cylindrical domains of PS–PMMA diblocks via tuning of interfacial energy[17]. However, this surface-modification process is restricted to homogeneous oxide surfaces, which presents some limitations, especially when commercial applications are considered. The Russell group observed perpendicular orientation of cylinders at high concentrations of chloroform in the film where the solvent was able to mediate interfacial interactions sufficiently to prevent the preferential segregation of one of the blocks to the surface[12]. However, the effectiveness of the solvent vapor approach is reliant upon the solvent quality with all the components. Furthermore, the method requires complicated experimental controls, which may not be feasible for industrial use. For these reasons, thermal annealing is more useful and attractive. However, due to the surface energies between different blocks and preferential affinities between one of the block, parallel cylindrical microdomains are always produced during thermal annealing.

Based on above, our objective here is to investigate i) the formation kinetics of SEBS interfacial layer on solid substrate and ii) the effect of interfacial sublayer with different composition on ordering the SEBS microdomains.

Chapter 2 Experimental Section

2.1 Sample Preparation.

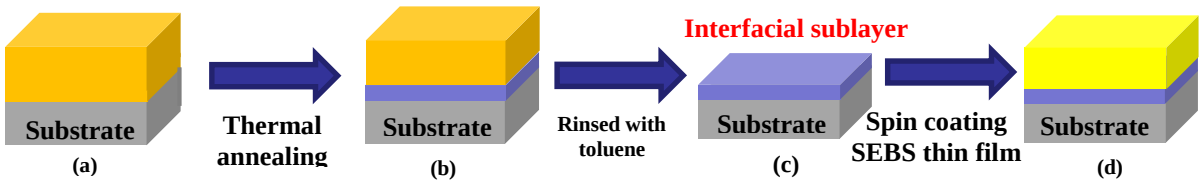

Scheme 1. Sample preparation process used in experiment

Poly (styrene-block-ethylene-butadiene-block-styrene) (SEBS) asymmetric block copolymer, with the weight average molecular weight (M_w) of 85,000 was obtained from Asahi-Kasei Chemical Corp. The weight fraction of the PEB component was 0.82, indicating cylindrical domains. The cylindrical forming of the bulk SEBS polymer within a wide range of temperature (25 °C – 180 °C) was further verified via in-situ small angle x-ray scattering carried out at X27C beamline at the National Synchrotron Light Source (NSLS) in Brookhaven National Laboratory (BNL) (Supporting information). Si substrates were cleaned by immersion in a hot piranha solution (i.e., a mixture of H_2SO_4 and H_2O_2, *caution*: the *piranha solution* is highly *corrosive* upon contact with the skin or eyes and is an explosion hazard when mixed with organic chemicals/materials; Extreme care should be taken when handing it.) for 15 min, subsequently rinsed with purified water thoroughly, and followed by submersion in an aqueous solution of hydrogen fluoride to remove native oxide. As been reported previously, a layer of SiO_2 with thickness about 1.3 nm was reproduced even after hydrofluoric acid etching due to atmospheric oxygen and moisture. SEBS thin films with average thicknesses $h = nL_0$, where L_0 is the domain spacing of the cylinders and n is an integer, were prepared by spin coating SEBS/toluene solutions onto H-Si substrates.

The scheme of sample preparation is shown in Scheme 1. The thickness of the spin-cast SEBS thin films was measured by an ellipsometer (Rudolf Auto EL-II) with the fixed refractive index of 1.516. The surface tension of PS block and PEB block are 40.6 mJ/m^2 (the dispersion part is 34.5 mJ/m^2 and the polar part is 6.1 mJ/m^2) and 42.2 mJ/m^2 (the dispersion part is 42.2 mJ/m^2 and the polar part is 0 mJ/m^2), respectively. based on the Owens-Wendt-Kaelble equation[18] with the dispersion part (48.71 mJ/m^2) and polar part (3.98 mJ/m^2) of the surface tension of bare H-Si[19], the interfacial energy (γ) of PS/H-Si and PEB/H-Si are then estimated to be 5.5 and xxx mJ/m^2, respectively. Thus, the PS block is believed to have more favorable interaction with the H-Si compared to the PEB block. All the spin-cast films were thermally annealed at 150 °C for different times in an oil-free vacuum below 10^{-3} Torr.

To investigate the irreversible adsorption of SEBS chains at the solid-polymer-melt interface, the thermally annealed samples were leached in baths of a fresh toluene at room temperature until the resultant film thickness remained constant. According to previous studies, anchored PS chains cannot be removed with this mild leaching condition, even they are only loosely adsorbed. Hence, this leaching condition is optimized to observe the formation of the SEBS loosely adsorbed layer (or the so called interfacial sublayer) which including both the outer loosely adsorbed chains and the inner flattened chains. The resultant SEBS adsorbed layers were dried in a vacuum oven at 150 °C for 12 h to remove any excess solvent trapped in the films before further experiments.

2.2 Grazing incidence small angle X-ray scattering (GISAXS)

Grazing incidence small angle X-ray scattering (GISAXS) measurements were carried out at X9 beamline at the National Synchrotron Light Source (NSLS) in Brookhaven National Laboratory (BNL). Two dimensional scattering patterns were collected using a MAR-CCD area detector with a sample-to-detector distance of 4950 mm. In order to see the differences in the microdomain structures between the topmost surface and the rest of the film, the two different incident angles (α) were utilized: (i) $\alpha = 0.06°$, which is just below the critical angle (α_c) of the total external reflection for SEBS ($\alpha_c = 0.1°$ with an X-ray energy of 13.5 keV used in this study) such that the electric field intensity decays exponentially into the film and thereby scattering intensity is dominated by the surface area of ~ 9 nm depth; (ii) $\alpha = 0.14°$, above α_c , where the X-ray penetration depth exceeds the film thickness such that we can obtain information on average structures over the entire film. We denote the first experimental configuration as the “surface-

mode" and the second one as the "film-mode" hereafter. All the measurements were carried out under vacuum which was in an order of 10^{-3} Torr with a temperature-controlled sample stage interfaced with a Lakeshore 340 unit. The exposure time was fixed at 200 sec and we confirmed no X-ray damage on the samples with such condition.

2.3. X-ray Reflectivity (XR) Measurements.

The x-ray reflectivity (XR) measurements were conducted at the X20 beamline (NSLS, BNL) to study the structures of the adsorbed SEBS layers on H-Si substrates after the solvent-leaching process. The specular reflectivity was measured as a function of the scattering vector in the

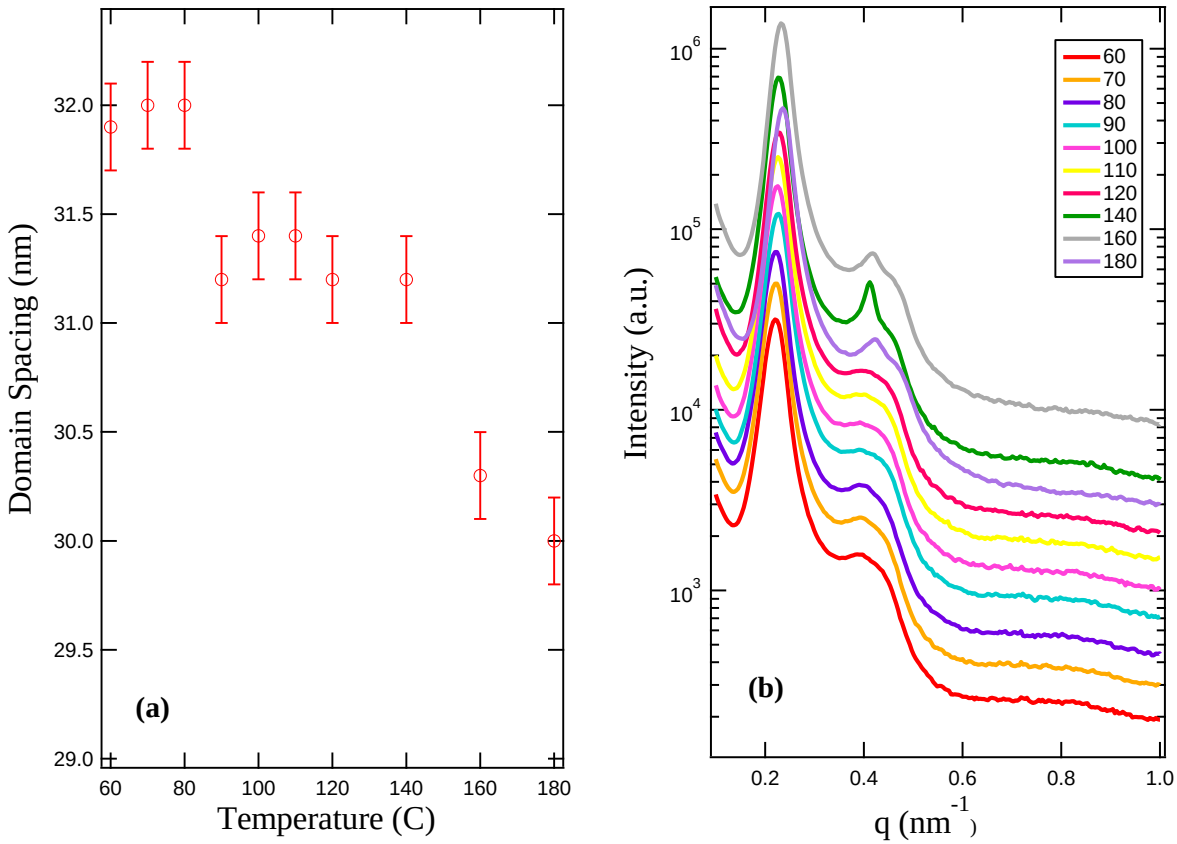

Figure 8. GISAXS data of SEBS bulk polymer. (a) domain spacing change (b) GISAXS 1D data with increasing of temperature from 60 °C to 180 °C.

perpendicular direction to the film surface, $q_z = (4\pi\sin\theta)/\lambda$, where θ is the incident angle and λ is

the x-ray wavelength (0.118 nm). The XR data was fit by using a standard multilayer fitting routine for a dispersion value (δ in the x-ray refractive index) in conjunction with a Fourier method, a powerful tool to obtain detailed structures for low x-ray contrast polymer multilayers[20]. Note that δ is proportional to the density of a film. For the x-ray energy at X20A (10.5 keV), the δ value of the bulk SEBS is estimated to be $\delta_{bulk} = 1.96 \times 10^{-6}$ with the density of 0.95 g/cm^3.

2.4. Atomic Force Microscope (AFM) measurements.

The surface morphology of the SEBS thin films was studied by atomic force microscope (AFM) (Digital Nanoscope III). The standard tapping mode was conducted in air using a cantilever with a spring constant of ~40 N/m and a resonant frequency of ~300 kHz. The scan rate was 1.0 Hz with the scanning density of 256 or 512 lines per frame.

Chapter 3 Result and discussion

3.1 Adsorption kinetics of SEBS interfacial sublayer.

As our group illustrated, the adsorption kinetics for homopolymers showed two stages which have first stage of power- law growth then switch to slow logarithmic growth and then reach a platuae state. Fig. 9 (b) shows the thickness of the PS and PB interfacial sublayers (h_f) measured by XR against t_{an}. From the figure we can see the PS and PB interfacial sublayer all exhibits power-

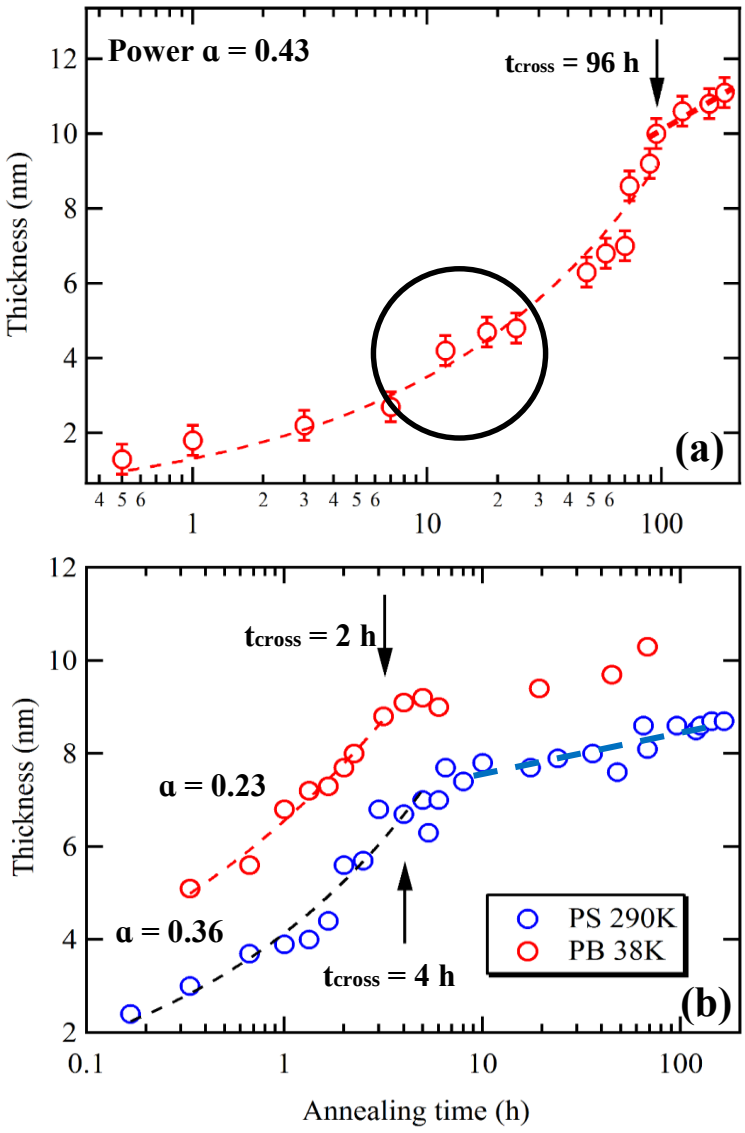

Figure 9. Formation of SEBS interfacial sublayer compared to that of PS and PB homopolymer: (a) shows SEBS interfacial sublayer, (b) shows PS and PB interfacial sublayer; respectively.

law growth ($\boldsymbol{h_f \propto t_{an}^{\alpha}}$) with $\boldsymbol{\alpha_{PS}}$= 0.36 ± 0.05 and $\boldsymbol{\alpha_{PB}}$=0.23 ± 0.05 at the early stage of the kinetics and there is a crossover time (t_c) at around 4 h for PS and 2 h for PB, where the power-law behavior

gives way to a slower logarithmic growth, followed by a plateau region at $t_{an} > 96$ h for PS. The overall adsorption kinetics of the interfacial sublayer is in good agreement with previous experimental results on the adsorbed PS monolayers on Al substrates[21]. However, comparison between the adsorption kinetics of SEBS block copolymer and PS or PB homopolymer shows clear difference. Figure 9 (a) shows the growth of interfacial sublayer of SEBS with increasing the annealing time, time for SEBS block copolymers to reach a quasiequilibrium adsorption seems to be much longer than that for the similar homopolymers (PS or PB) with comparable molecular weight on the same solid substrate, possibly due to the complication in the chain architecture which makes the relaxation and re-arrangement of adsorbed chains become more sluggish. However, if we carefully look at the adsorption kinetics, it seems that the growth of the SEBS interfacial sublayer can be also divided into three kinetic stages (as shown in Fig. 2) with two different power law growth ($0 \text{ h} < t_{an} < 12 \text{ h}$ and $12 \text{ h} < t_{an} < 90 \text{ h}$) at the early stage before transfer into logarithmic growth (reaching the t_c). This result is very similar to the one reported by Eskilsson and Tiberg,[3] who show that the adsorption of triblock copolymers from solution is constitute of three stages instead of the two-stage adsorption found in homopolymer systems.[22] They propose the additional stage taken place in between the early stage (with low surface coverage) and the final logarithmic regime (with high surface coverages) is arise from the displacement between the different anchored blocks in the adsorbed copolymers which have different interaction with the substrate. However, as will be shown later, during the intermediate adsorption process, the resultant interfacial sublayer is so heterogeneous at the surface due to the formation of micelle structures that the use of ellipsometry or x-ray reflectivity may not be accurate enough to determine the thicknesses of the

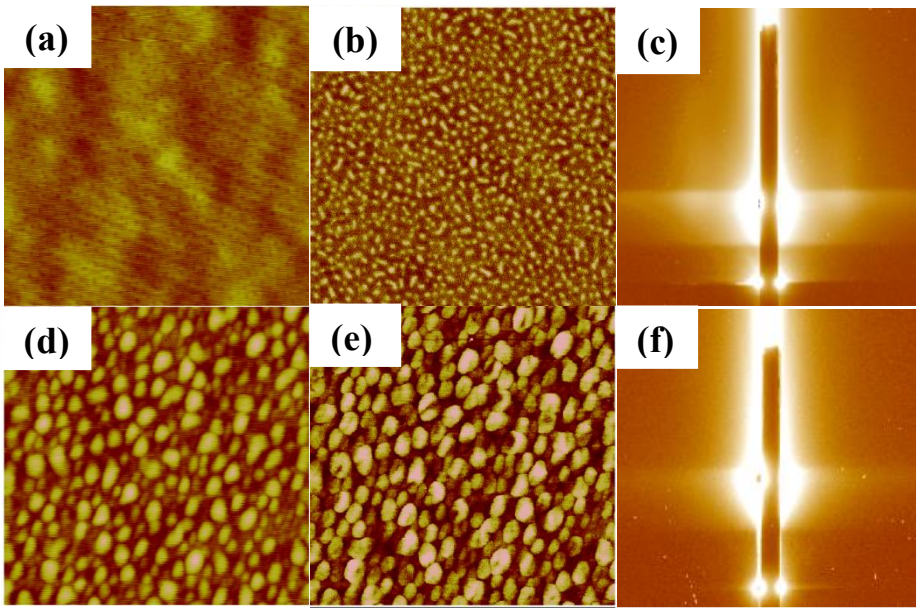

Figure 10. Surface morphology of SEBS interfacial sublayer and flattened layer: (a) and (b) show AFM height and phase image and (c) shows GISAXS data of interfacial sublayer; (d) and (e) show AFM height and phase image and (f) shows GISAXS data of flattened layer. The scales are all 1um for AFM images.

transient interfacial sublayers. Two kinds of solvent are using to obtain SEBS interfacial sublayer and flattened layer, which are toluene and chloroform. Morphology of SEBS interfacial layer and flattened layer are shown in Figure 10, the thickness are roughly 10 nm and 2.5 nm, respectively. From phase image of interfacial sublayer (shown in Figure 10 (b)), PS cylinder normal to the surface can be observed, which indicates that loosely adsorbed SEBS chains can phase separate into cylindrical microdomain, but the cylinder microdomain does not follow very good order. While for SEBS flattened layer, shown in Figure 10 (d) - (f), there is no phase separation observed. This is confirmed by both AFM and GISAXS results. Instead, the quasiequilibrium SEBS flattened layer shows dimple-like structures with a characteristic length of several tens of nanometers and a surface coverage of ~ 55 % at the surface. It may because all the copolymer chains strongly pining onto the substrate so that phase separation is hindered. This is proved by both the cross sectional analysis of the height image and the scratch test using a razor blade. The surface feature of SEBS flattened layer is very similar that of homopolymer flattened layers on silicon substrate as has been reported previously,[23] which shows the substrate surface are not fully covered by the flattened chains due to the relatively weak polymer-substrate interaction. The lack of cylindrical

microdomains structures in the 2.5 nm-thick flattened layer is possibly due to the presence of many solid/segment contacts which prevents the formation of SEBS cylindrical microdomains near the substrate interface.

3.2 How does SEBS interfacial sublayer form?

The time evolution of the surface morphologies of SEBS interfacial sublayers measured by tapping-mode AFM is shown in Figure 11. With short annealing time, cylindrical domains were only partially formed at the surface of the transient interfacial sublayer with the cylinders aligned normal to the substrate. As more SEBS chains further reel-in and adsorb to the H-Si substrate, micellar structures with several hundred nanometers in average diameter were formed at the surface with the minor PS-blocks aggregated at the surface of these micelles (based on the phase contrast from the AFM images). This can also be confirmed by Green et al[24], who reported that when the surface energies of two blocks are similar, the copolymer with longer chains shows stronger tendency to aggregate to form micelles than do the short chain copolymer. With increasing annealing time, the amount of micelles per unit area increases accompanied by the increase of the

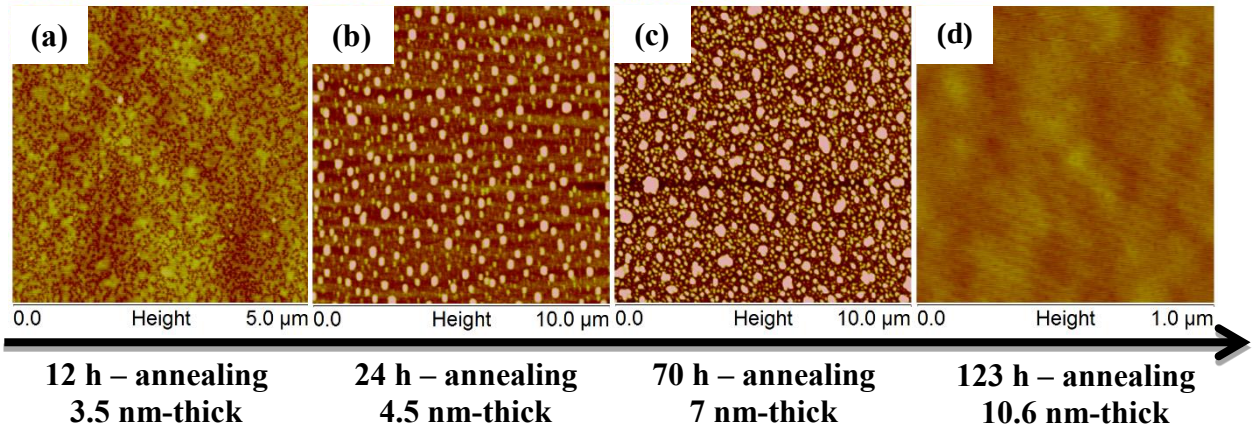

Figure 11. AFM height image of SEBS interfacial sublayer annealing for different time. Color bar is -10nm~ 10nm, scale bar is shown.

thickness of the interfacial sublayer. After reaching the crossover time t_c, the interfacial sublayer become comparatively smooth and cylindrical standing microdomains were appeared evenly at the surface. The enhancement in the ordering of SEBS microdomains of the interfacial sublayer from

the transient state to the quasiequilibrium stage was also confirmed by the one-dimensional GISAXS results. It should also be mentioned that although the thickness of interfacial sublayer still grows extremely slowly after t_c, the surface morphology and the ordering of cylindrical microdomains of these mature interfacial sublayers with thickness ranging from 10 – 11 nm remained almost the same. However, based on the GISAXS results and the Fourier transformation of the AFM images, we found that the standing cylinders are poorly aligned in the lateral direction in the quasiequilibrium interfacial sublayer. And a well-ordered hexagonally closed packed configuration cannot be achieved even we thermally annealed the 10 nm-thick interfacial sublayer at high temperatures for extremely long time. This is likely arise from the strong pinning of SEBS adsorbed chains on the silicon substrate which limited the polymers to recover their bulk-like microdomain configuration (ordering). (Besides, the domain size of PS in the SEBS interfacial sublayer is estimated to be 12 -15 nm, much less than that in 25 nm-thick films (22 nm), this may arise from the additional entropic penalty of stretching the adsorbed chains which affects the separation of PS and PEB microdomains.)

On the other hand, the SEBS flattened chains did not form any cylindrical microdomain structures at the substrate interface including both the transient state and the final quasiequilibrium state (with thickness ranging from 1 nm to 2.5 nm). This is confirmed by both AFM and GISAXS results (see supplemental results). Instead, the quasiequilibrium SEBS flattened layer shows dimple-like structures with a characteristic length of several tens of nanometers and a surface coverage of ~ 55 % at the surface. This is proved by both the cross sectional analysis of the height image and the scratch test using a razor blade. The surface feature of SEBS flattened layer is very similar that of homopolymer flattened layers on silicon substrate as been reported previously,[23] which shows the substrate surface are not fully covered by the flattened chains due to the relatively weak polymer-substrate interaction. The lack of cylindrical microdomains structures in the 2.5 nm-thick flattened layer is possibly due to the presence of many solid/segment contacts which prevents the formation of SEBS cylindrical microdomains near the substrate interface. However, in case of the interfacial sublayers (3.5 to 11 nm in thickness), the outer adsorbed chains, which are lately arrived during the adsorption process, are more loosely attached due to the limited available empty sites at the solid surface. As a results, these loosely attached chains have more freedom in phase separate into SEBS microdomain structures compared to the flattened chains. The above findings are analogue

to the one found in our very recent report which shows that the 2.5 nm-thick PEO flattened chains could not crystallize on the silicon substrate while the loosely adsorbed PEO chains are still able to crystallize via the so called diffusion limited aggregation process.

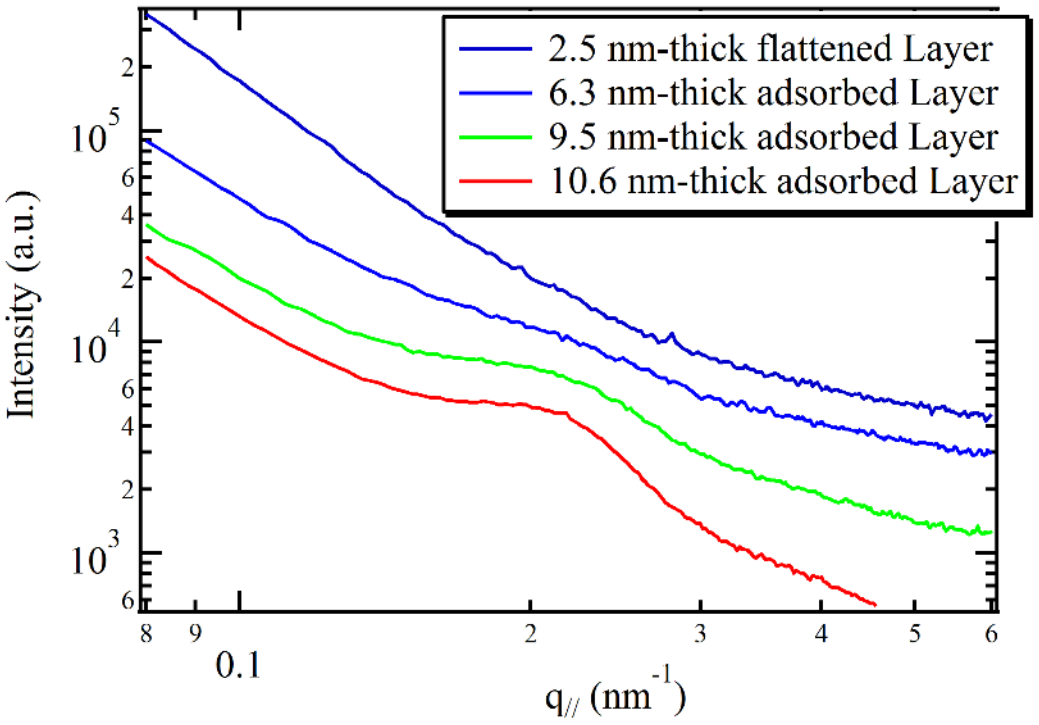

Figure 12. 1D GISAXS data of SEBS adsorbed layer with different annealing time.

To better understanding of formation of SEBS adsorbed layer, cartoons in Figure 12 can help. At first, all the blocks, regardless of interaction with substrate, adsorb on the substrate and form flattened chain conformation at the surface. At this time, there are many empty space at the surface so that the surface is heterogenous. With time increasing, more and more copolymer chains come

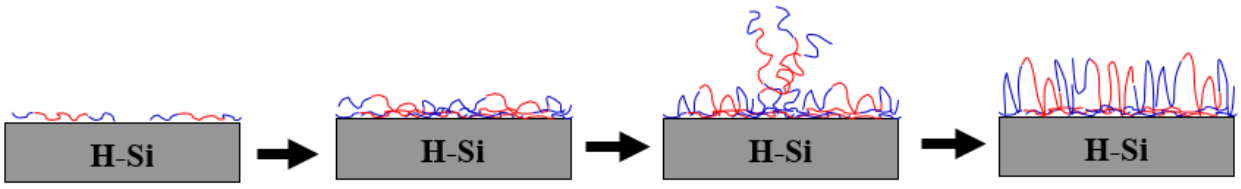

Figure 13. Formation of SEBS adsorbed layer on silicon substrate.

to the surface and started to overlap each other. The surface becomes homogenous and shows cylinder mircodomains. When more and more copolymer chains overlap with each other, PS block started to form a cluster which stay away from surface since PB block has more favorable interaction with the substrate. At this moment, PS microdomain can be seen, as shown in Figure 11. After very long time annealing, cylindrical microdomains can be obtained and the surface become homogenous.

3.3 Samples prepared on Si substrate.

Fig. 14 (a) – (f) shows the surface morphology of 25 and 75 nm-thick SEBS film prepared on H-Si substrate after thermally annealed at 150 ºC for three different times, 3 h, 96 h, 186 h, respectively. Preferrentially perpendicular cylinders were formed for the 25 nm-thick film with the diameter of the cylindrical domains d = 22.2 ± 1 nm. The minimum center-to-center distance between cylindrical microdomains was estimated to be 25.3 ± 1 nm based on the cross-sectional analysis of the phase images. However, the Fourier transformation of the AFM phase image suggests that these cylinders are not well hexagonally packed on the silicon substrate. From the annealing time dependece, we can see that the bulk-like hexagonal packing of cylinders cannot be achieved even thermally annealed at 150 ºC for extremely long time. As the film thickness increase ($h > L_0$), long strands of the minor block PS arranging parallel with respect to the surfaces were observed, indicating the orientation of the cylindrical microdomains then changed from perpendicular to parallel at the polymer-air interface. Such transition in cylindrical microdomains is likely due to the selective nature of the polymer−surface interactions: one block has a preferential attraction with either the H-Si substrate or the air interface (i.e. the PS block which has relatively lower surface energy compare to the PEB block). However, parallel cylinder seems unfavorable in 25 nm-thick film likely because of the incompatibility between the lattice spacing of the microdomains and the film thickness. (The formation of perpendicular oriented cylinders within the 25-nm thick SEBS film indicate that there is no strong preferential interaction between either block of the SEBS with the H-Si surface.)

On the other hand, the surface morphology of 75 nm-thick film is almost independent of the annealing time with relatively small grain size of the microdomains and poor orientational ordering, indicated by the presence of non-parallel laying cylinders. Fig. 15 shows the film-mode one - dimensional GISAXS patterns of the SEBS film corresponding to the samples in Fig. 14 (d) to (e), respectively. The change in the GISAXS pattern clearly show that the cylindrical microdomains does change within the film as a function of annealing time. For the sample annealed for 96 h, we observed clear ring-like scattering from the reflected beam with a maximum peak at

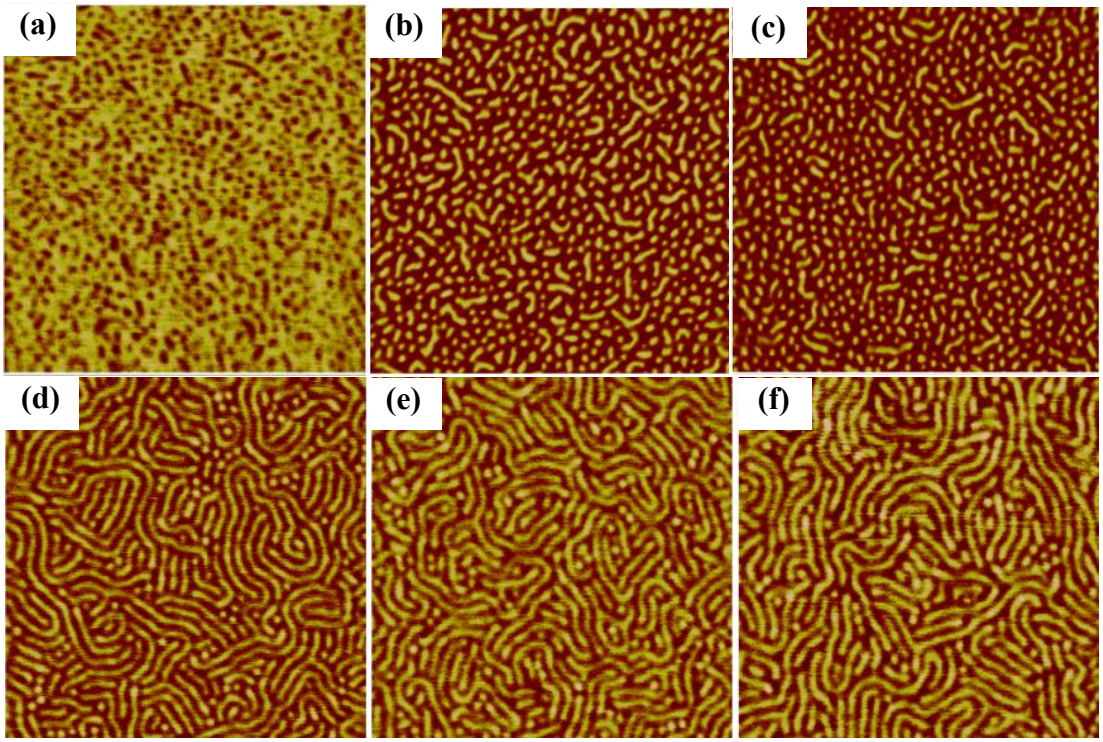

Figure 14. AFM phase images of SEBS 25 nm and 75 nm thin films prepared on Si substrate after certain times of annealing at 150 °C; (a) – (c) show 25 nm thin film annealed for 3h, 96h and 186h, respectively; (d) – (f) show 75 nm thin film annealed for 3h, 96h, 186h, respectively.

$q = 0.248\ nm^{-1}$, which corresponding to the distance between adjacent cylinders we estimated from Figure 14 (a). At the same time, rod-like shape (stripes) scattering patterns along the q_z direction with constant q_{xy} value were also observed in the same 2D image (not shown here). These data indicate that within the 75 nm-thick film, a portion of the cylinders stand perpendicular to substrate, while at the same time, the rest of the cylinders were randomly aligned without a specific of orientation. The gradually increase in the sharpness of the first and second order reflection peaks indicate that the SEBS cylinders are re-arranging themselves into a more ordered state upon

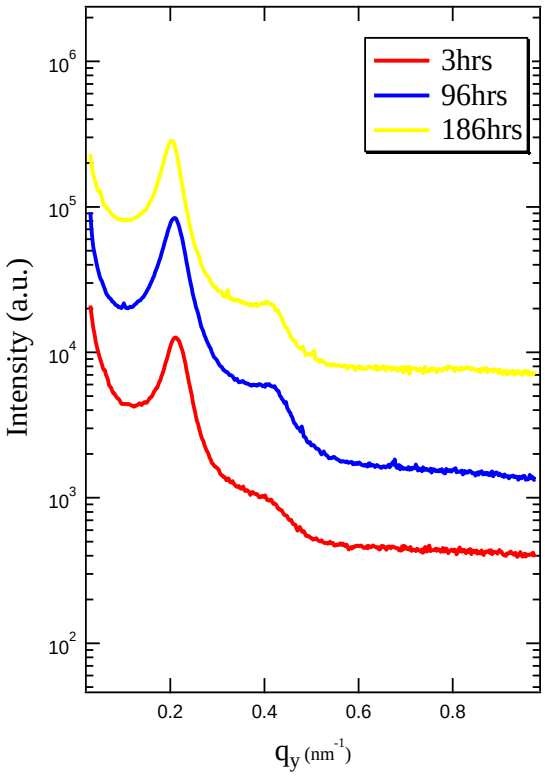

Figure 15. 1D GISAXS data of SEBS 75 nm thin film prepared on bare silicon substrate after annealed for 3h, 96h and 186h at 150 °C.

annealing. However, the ordering dynamics is extremely slow even at 150 ºC, a temperature far above the bulk Tg, and an equilibrium state of ordering is not achieved within the experimental time scale. Combine with the annealing time independent AFM results, it is obvious that the slow re-arrangment of the cylindrical microdomains is not likely taken place at the very polymer-air interface, but happening in either the interior of the film or the polymer-substrate interface.

Although prolong annealing time will make more cylinder lie down from the surface because of surface effect, after longer annealing time, the string which indicates standing cylinder

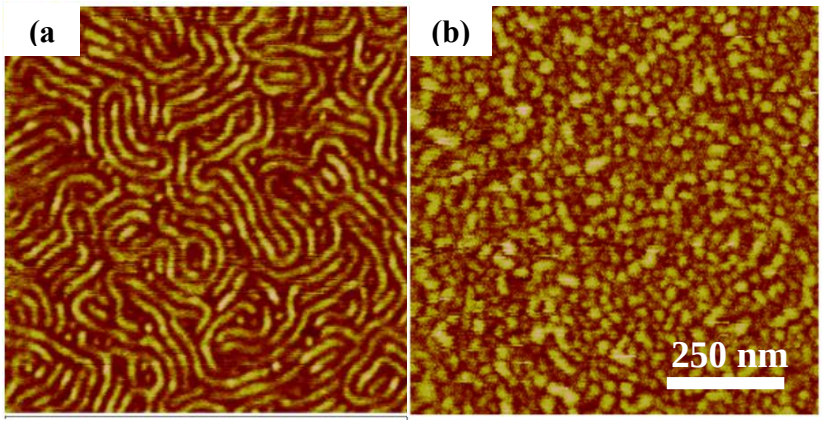

Figure 16. AFM images of SEBS 80nm thin films prepared on bare silicon substrate annealed for 96 h with (b) and without (a) 5 minutes oxygen plasma etching. The scale bar is 250 nm.

microdomain becomes more intense. 1D GISAXS data in Figure 14 shows that with annealing time increasing, cylindrical microdomains become more ordered, which can be seen in the

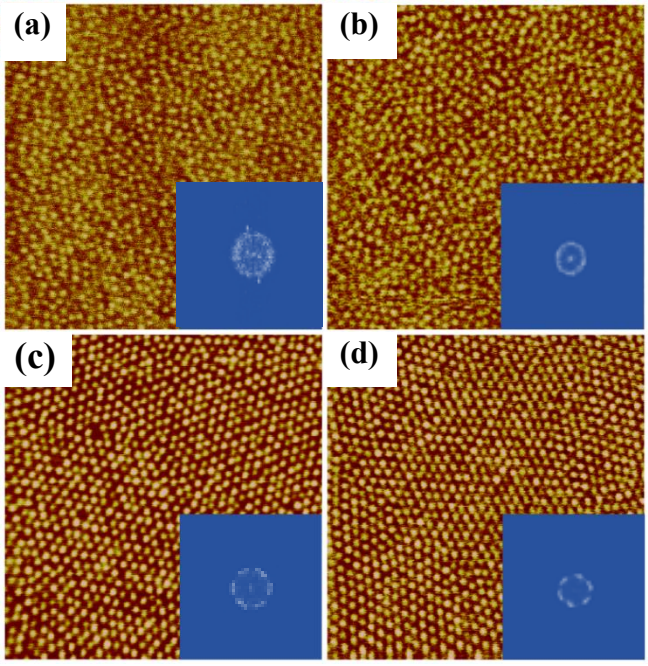

Figure 17. AFM images of 25 nm SEBS thin films prepared on (a) bare silicon, (b) SEBS interfacial sublayer, (c) PB interfacial sublayer, (d) PS interfacial sublayer. Scale bar is 1 um. Insets are Fourier Transmisson data.

presence of second order peak. So the cylindrical micodomain become ordered from the bottom.

To further investigate the effect of adsorbed layer on microdomains, three different interfacial sublayer were used, which are SEBS, PS and PB interfacial sublayers. 25nm thick SEBS thin film

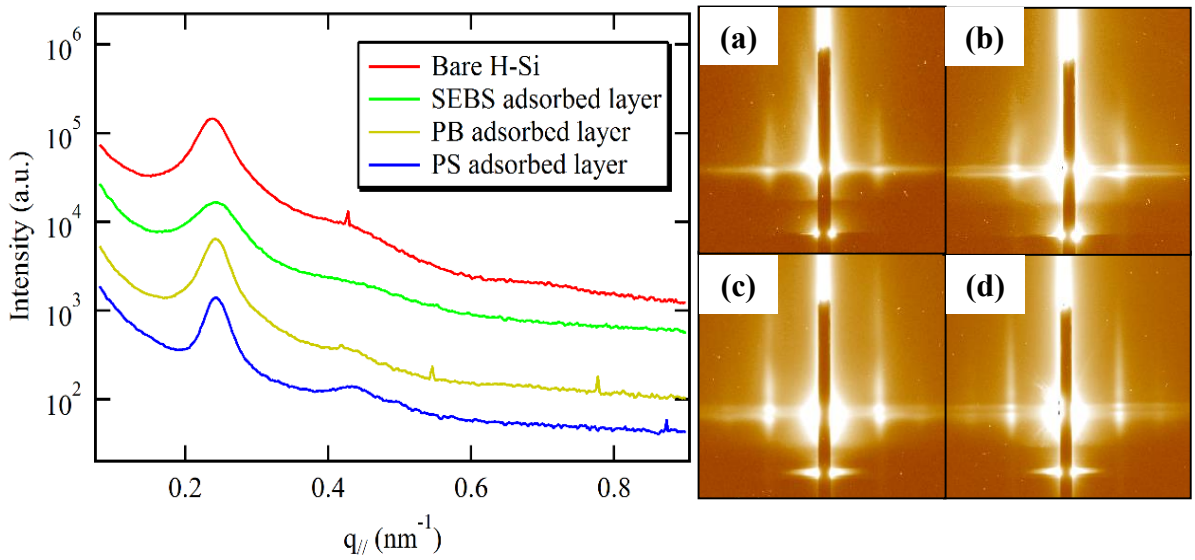

Figure 18. GISAXS data of 25nm SEBS thin films on different substrate: (a) on bare silicon, (b) on SEBS adsorbed layer, (c) on PB adsorbed layer, (d) on PS adsorbed layer.

were spun cast on bare silicon, SEBS interfacial sublayer, PB interfacial sublayer and PS interfacial sublayer. AFM images as well as FT images were shown in Figure 16. On bare silicon and SEBS interfacial sublayer, the cylindrical microdomains are not well ordered. While when SEBS was spun cast on PS and PB interfacial sublayer, perfect hexagonal cylindrical microdomains can be observed. The reason for this phenomenon may due to the natural of homopolymer interfacial sublayer. Interfacial sublayer of homopolymer consists of two layers with different chain conformation: flattened chains that constitute the inner higher density region of the adsorbed layers and loosely adsorbed polymer chains that form the outer bulklike density region. Loosely adsorbed chains can entangle with other polymer chains which are above this region. However, the polymer chains of thin films do not adsorb on the substrate, which enable them to

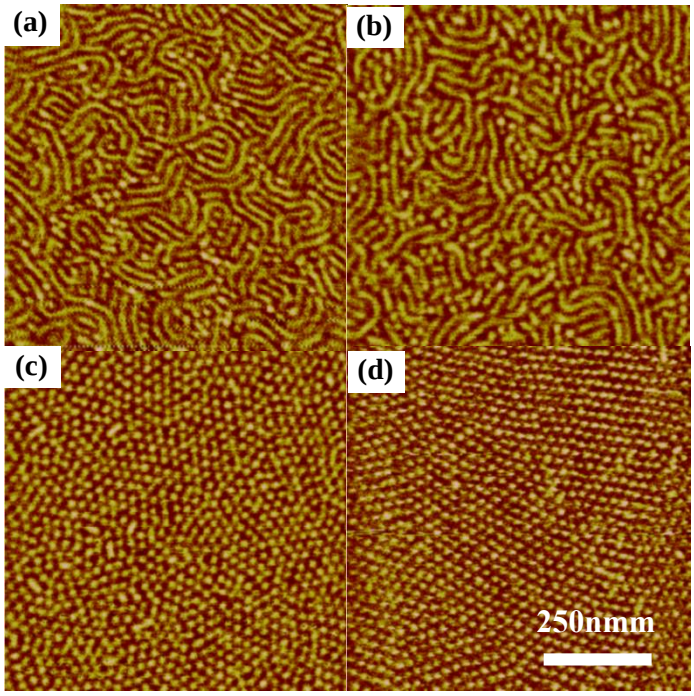

Figure 19. AFM phase image of 50 nm thick SEBS thin film spun cast on different substrate: (a) on bare silicon, (b) on SEBS interfacial sublayer, (c) on PB interfacial sublayer, (d) on PS interfacial sublayer. The scale bar is 250 nm.

have more mobility so that they can have nice phase separate. However, for SEBS thin film on SEBS interfacial sublayer, things are different. SEBS interfacial sublayer has cylindrical

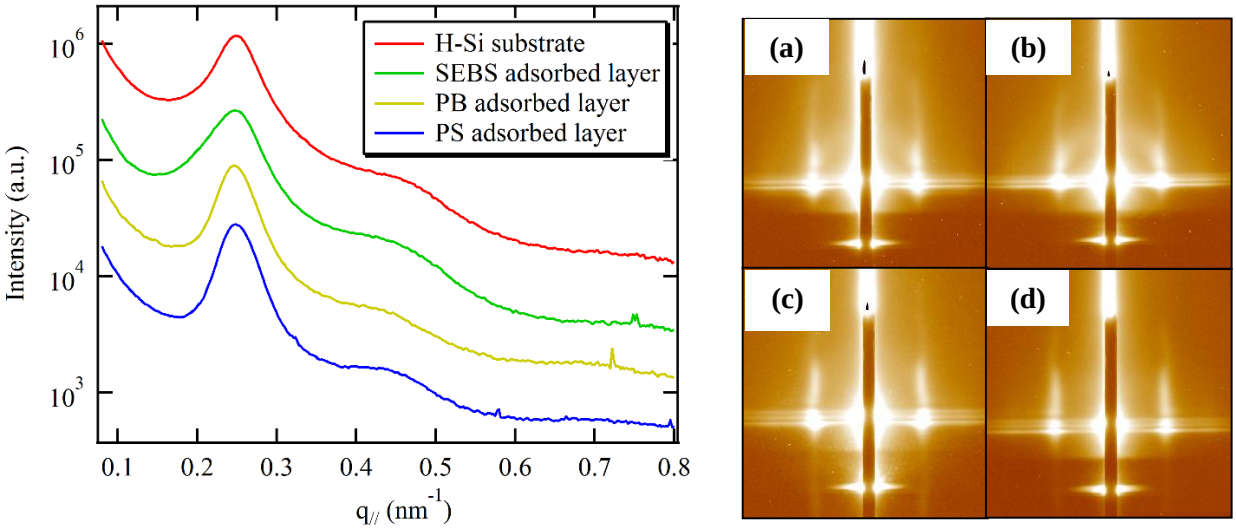

Figure 20. 1D GISAXS data of 50 nm SEBS thin film prepared on different substrate shows in left hand side, 2D GISAXS data of (a) bare silicon, (b) SEBS interfacial sublayer, (c) PB interfacial sublayer, (d) PS interfacial sublayer as substrate show on right hand side.

microdomains itself as shown in Figure 9. So when spin casting SEBS thin films on top, the bottom patterned structure will affect phase separate of top film, resulting in random cylindrical microdomains normal to the surface. GISAXS data of SEBS thin films on different substrate were shown in Figure 15. It can be clearly seen that on PB and PS interfacial sublayer, cylindrical microdomains are perfectly packed and the strings in Figure 19 (c) and (d) are much longer than that in (a) and (b). Right side 1D data shows second order peak for SEBS thin films on PS and PB interfacial sublayer.

What will happen if thicker film (d>$\boldsymbol{L_0}$) were spun cast on these different substrate? Previous works have shown that cylinder microdomains normal to the surface can only be obtained when the thickness of thin film is around domain spacing. 50nm (d = 2$\boldsymbol{L_0}$) were spun cast on these four substrates, AFM images are shown in Figure 20. For thicker film, cylindrical microdomain started to be parallel to the substrate from the surface on bare silicon as well as on SEBS adsorbed layer. However, for PB and PS interfacial sublayer, SEBS thin films on top still form perfect hexagonal cylinder microdomains. This result has great agreement with our hypothesis which is homopolymer interfacial sublayer can be used as a neutral interface between polymer and substrate to eliminate the adsorption of polymer chains so that copolymer can easily phase separate into perfect cylinder microdomains regardless of film thickness. GISAXS data was shown in Figure 21. For SEBS 50nm film on SEBS and silicon substrate, shown in Figure 21 (a) and (b), the strings are not very straight and there are "rings" forming which indicating random orientation of

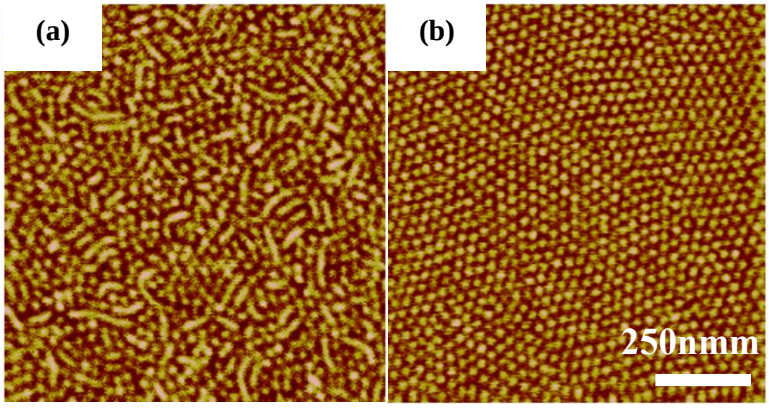

Figure 21. AFM phase images of 100 nm SEBS thin film on PB (a) and PS (b) interfacial sublayer, scale bar is 250nm.

cylinders (mixture of parallel and perpendicular cylinders). While on PS and PB interfacial

sublayer, there are only straight strings and a blurry second order peak, which indicate well-ordered cylinder microdomains through the film.

Although the loosely adsorbed SEBS chains can microphase separate into cylindrical microdomains, the lateral long-range ordering is poor and cylinders are not well hexagonally packed due to the presence of surface-segment contacts. As a result, the SEBS melts in contact with the loosely adsorbed chains maintained the same lateral order as the adsorbed layer to ensure the continuity of cylindrical microdomains. And base on the GISAXS and plasma etching experiments, we found that the poorly ordered cylinders at the substrate interface can propagate at least 70 nm-thick into the film interior. However, when $h > L_0$, parallel cylinders are always formed at the very surface due to the segregation of PS blocks which has lower surface energy as compared to that of PEB. Since the segmental mobility has been found largely reduced near the substrate compared to the free surface due to the adsorption of polymer chains, it is reasonable to deduce that the parallel cylinders are already formed at the free surface before the formation of standing cylinders propagate into the surface region from the substrate. Hence, when the thickness is above 25 nm, the entire film is constituted of cylindrical microdomains with two different orientations competing each other: at the free surface, cylinders are lying parallel to the surface and develop into the film interior; near the substrate interface, perpendicular cylinders were formed and propagate into the film interior. Such heterogeneity in microdomain orientation is consistent with previous studies which show that both parallel and perpendicular orientation of microdomains may coexist in the film if either A or B blocks has preferential interaction at one interface and nonpreferential interaction at the other interface.[25]

Next question is how far the cylinders can stand from the homopolymer interfacial sublayer. 100nm ($d=3\boldsymbol{L_0}$) SEBS thin films were spun cast on PS and PB interfacial sublayer to explore the effect, results are shown in Figure 20. In Figure 21 (a), cylinders at the surface started to lie down due to surface effect on PB adsorbed layer. While in Figure 20 (b), perfect hexagonal packed cylindrical microdomains can be observed on PS interfacial sublayer.

3.4 High temperature effect on SEBS microdomains

Polymer chains can move under temperature above Tg. For block copolymers, the movement of

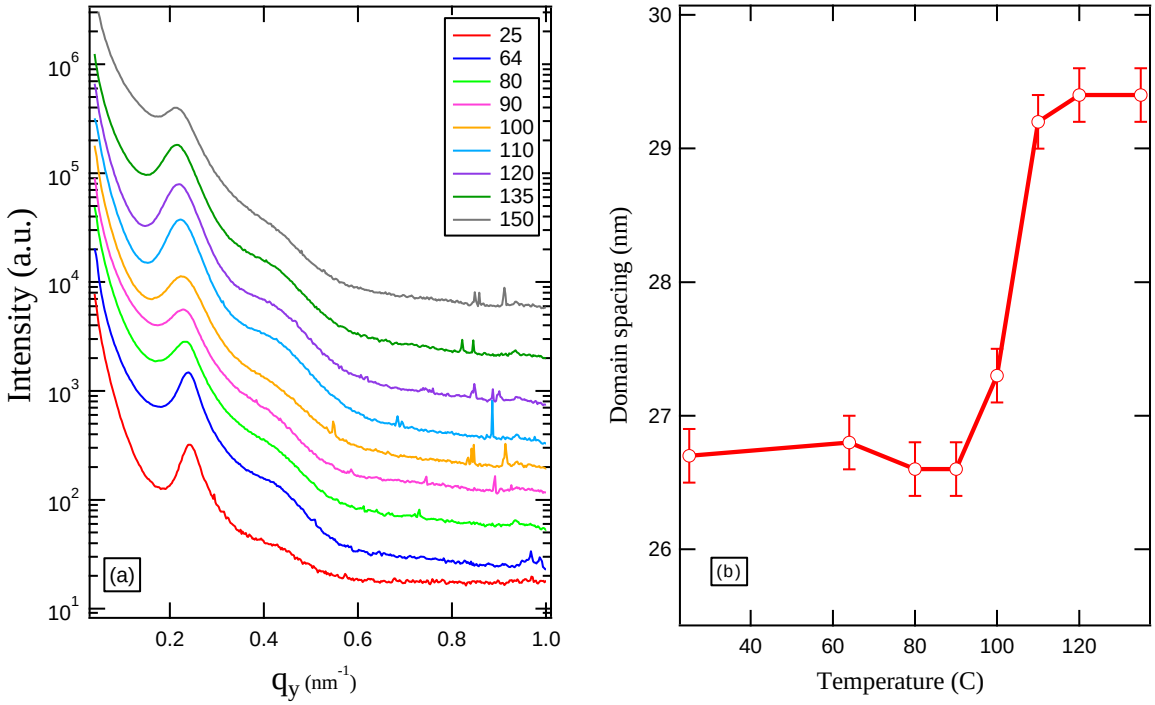

Figure 22. GISAXS 1D data (a) of different temperature and temperature dependence of domain spacing (b) of SEBS 25 nm thin film prepared on hydrogen-passivated silicon substrate.

polymer chain has significant effect on microdomains[26]. SEBS 25nm thick films prepared on different substrate (bare silicon, SEBS interfacial sublayer, PS 290k interfacial sublayer, PB interfacial sublayer) were chosen for high temperature GISAXS experiments. The temperature scale was 25 ℃ to 150 ℃. Figure 21 shows 1 dimensional GISAXS data of SEBS 25nm thin films on bare silicon. As temperature goes up, first order peak position gradually shifts towards smallerq_y, which means the domain spacing of SEBS microdomains become larger since $D \sim 1/q_y$. However, there is no obvious difference for the second order peak. This result shows great agreement with what Ham et al[27] have done. As shown in Figure 22, distance between two strings becomes smaller and two strings become unclear when temperature was around 90 °C which is Tg for PS.

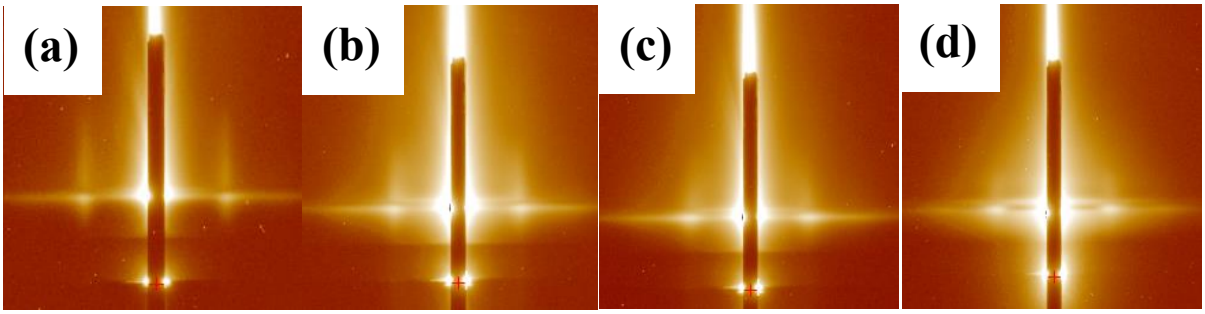

Figure 23. 2D GISAXS data of SEBS 25nm thin film on HSi at different temperature. (a) 25 °C, (b) 80 °C, (c) 100 °C, (d) 150 °C.

When prepared on SEBS interfacial sublayer, the results of SEBS thin film for the high temperature GISAXS experiment shows in Figure 23. The first order peak shown in Figure 23 (a) shifts towards smaller q_y as temperature goes from 25 °C up to 150 °C with a big shift when the temperature is around 85 °C. The curve in Figure 20 (b) shows the domain spacing change with

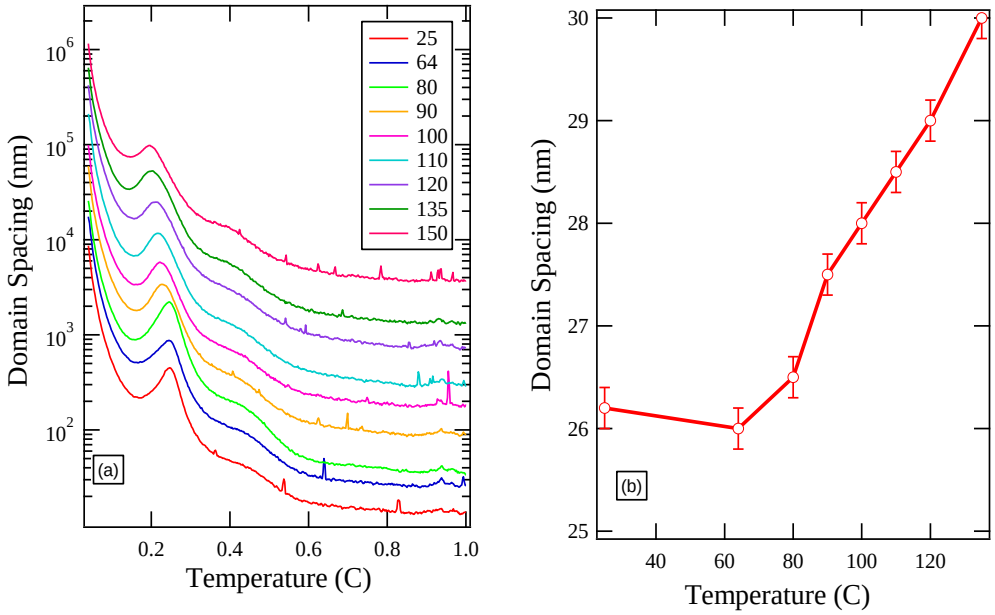

Figure 24. GISAXS 1D data (a) of different temperature and temperature dependence of domain spacing (b) of SEBS 25 nm thin film prepared on SEBS interfacial sublayer.

increasing temperature. We can see that domain spacing of SEBS thin film on SEBS interfacial sublayer increases when the temperature goes higher, which indicates that the mobility becomes higher at high temperature. Figure 24 shows the 2D GISAXS images of SEBS 25 nm thin film prepared on SEBS interfacial sublayer. As temperature increases, the strings which are

corresponding to first order peak in Figure 23 (a) become shorter and more unclear. Also the distance between two strings become smaller, indicating the domain spacing become larger.

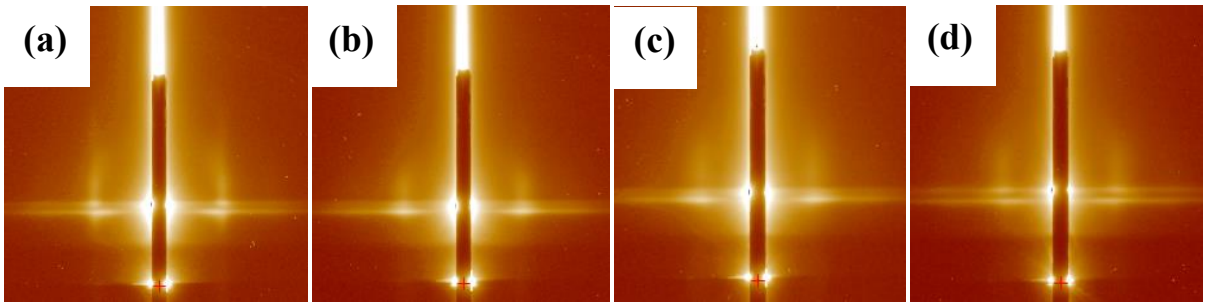

Figure 25. 2D GISAXS data of SEBS 25nm thin film on SEBS interfacial sublayer at different temperature. (a) 25 °C, (b) 80 °C, (c) 100 °C, (d) 150 °C.

GISAXS data of SEBS 25 nm thin film prepared on PB interfacial sublayer are shown in Figure 24. On the left hand side of Figure 24, 1D GISAXS data shows that with increasing the

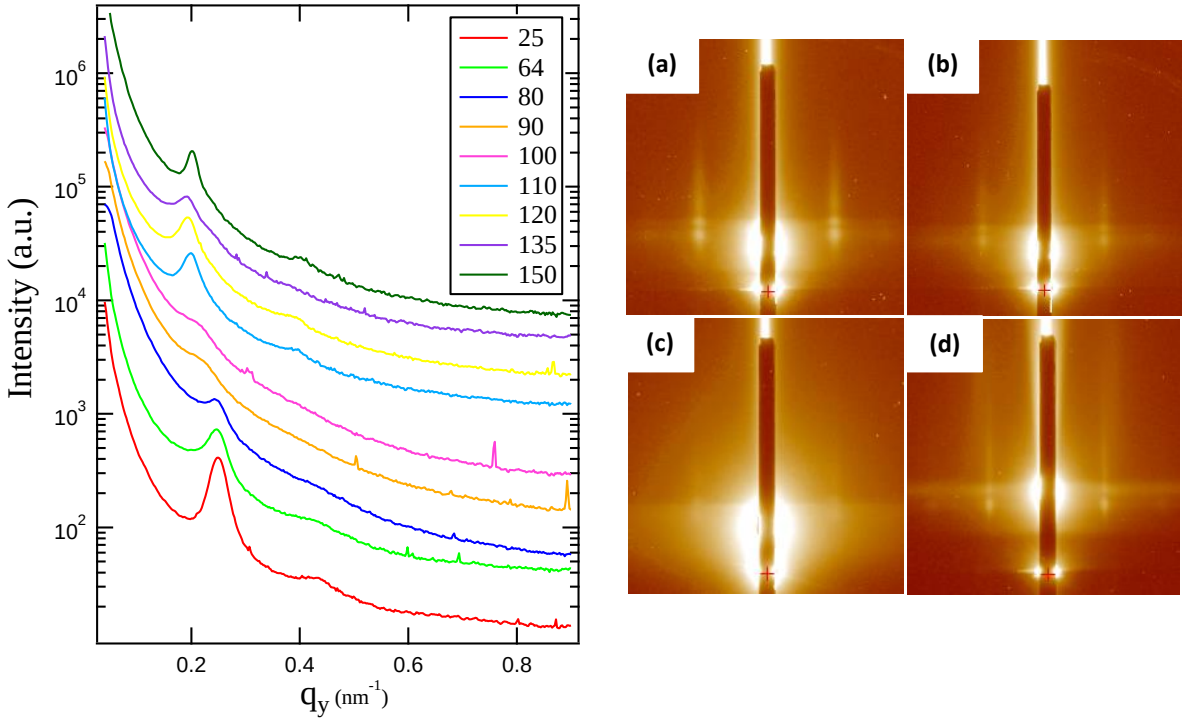

Figure 26. GISAXS 1D data of SEBS 25 nm thin film prepared on PB interfacial sublayer (left handside) and GISAXS 2D data of SEBS 25 nm film prepared on PB interfacial sublayer (right hand side) at different temperature : (a) 25 °C, (b) 64 °C, (c) 100 °C, (d) 150 °C.

temperature, the first order peak gradually disappears around 90 °C which should be the T_g of the SEBS block copolymer. When temperature goes above 100 °C, the first order peak appear again

with smaller width. There must be something happened but we are not sure yet. From the 2D GISAXS images on the right hand side, we can see the strings disappear at temperature around 100 °C, which shows good agreement with 1D data shown on the left. It is hard to fit the data for determine the position of first order peak since the peak is somewhat irregular.

It is known that if anneal longer time, cylinders will lie down from the surface. Also, if anneal longer, the morphology will get closer to equilibrium state. We here compare SEBS thin films spun cast on bare silicon and PS interfacial sublayer which are both annealed for very long time, shown in Figure 26. When spun cast on bare silicon, even anneal for 168h, the grain size of cylinder

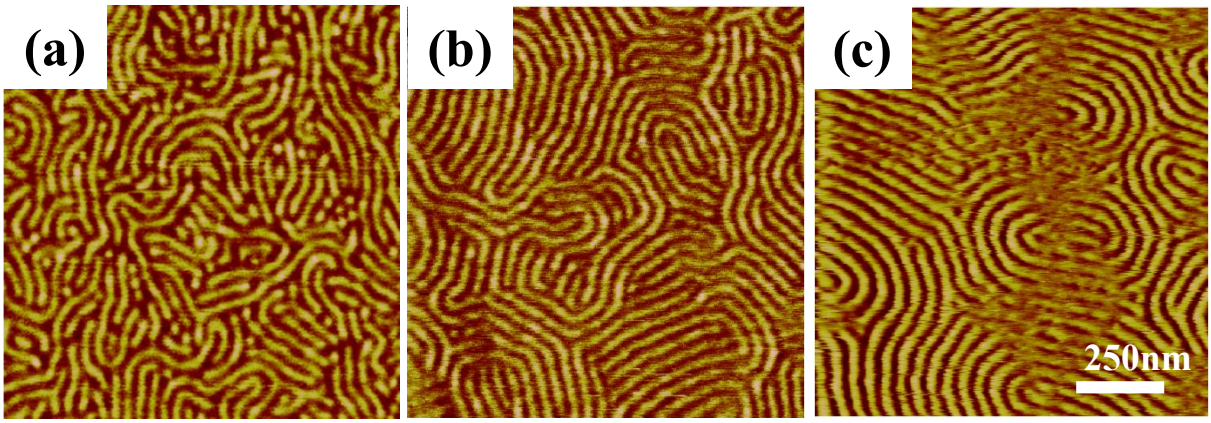

Figure 27. AFM phase images of 100nm SEBS film spun cast on bare silicon (a) annealed for 168h and on PS interfacial sublayer annealed for 96h (b) and 128h (c).

is smaller than that on PS adsorbed layer anneal for 96h and 128h. This result indicates that homopolymer interfacial sublayer can eliminate copolymer chain adsorption and accelerate phase separation, which is in agreement with previous research[28].

Chapter 4. Conclusion

When the film thickness is N times of the microdomain spacing, cylinders can stand from the bottom for block copolymers. In this thesis we show that the homopolymer interfacial sublayer could help ordering the cylindrical microdomain of block copolymers by eliminating the adsorption of block copolymer chains onto the substrates. We use AFM and GISAXS to confirm our hypothesis. And PS interfacial sublayer works best in this case. We prepared a variety of adsorbed layers composed of SEBS, polystyrene and polybutadiene homopolymers and studied the possibility to use them an alternative polymer coating materials in place of end-grafted polymer brushes. The experimental results clearly show that the morphologies of the SEBS ultrathin films on top of the adsorbed layer vary with a choice of the adsorbed layer: the PS adsorbed layer is the best to create well-ordered perpendicular cylindrical microdomain structures, while the SEBS adsorbed layer induces parallel cylindrical microdomain orientation instead. Hence, the present study proposes a new way to manipulate the orientation and degree of ordering of microdomain structures in BCP ultrathin films.

Reference

[1] Thomas P. Russell, Curr Opin Colloid In **1** (1), 107 (1996).

[2] M. W. Matsen, The Journal of Chemical Physics **113** (13), 5539 (2000).

[3] Krister Eskilsson and Fredrik Tiberg, Macromolecules **30** (20), 6323 (1997).

[4] Christopher Harrison, Paul M. Chaikin, David A. Huse, Richard A. Register, Douglas H. Adamson, Abishai Daniel, E. Huang, P. Mansky, T. P. Russell, Craig J. Hawker, David A. Egolf, Ilarion V. Melnikov, and Eberhard Bodenschatz, Macromolecules **33** (3), 857 (1999).

[5] Rachel A. Segalman, Materials Science and Engineering: R: Reports **48** (6), 191 (2005).

[6] Kataoka Kazunori, Kwon Glenn S, Yokoyama Masayuki, Okano Teruo, and Sakurai Yasuhisa, J. Control. Release **24** (1–3), 119 (1993); Christine Allen, Dusica Maysinger, and Adi Eisenberg, Colloids and Surfaces B: Biointerfaces **16** (1–4), 3 (1999).

[7] Elisa Martinelli, Sara Menghetti, Giancarlo Galli, Antonella Glisenti, Sitaraman Krishnan, Marvin Y. Paik, Christopher K. Ober, Detlef- M. Smilgies, and Daniel A. Fischer, Journal of Polymer Science Part A: Polymer Chemistry **47** (1), 267 (2009).

[8] J. Y. Cheng, C. A. Ross, E. L. Thomas, Henry I. Smith, and G. J. Vancso, Appl Phys Lett **81** (19), 3657 (2002); Miri Park, Christopher Harrison, Paul M. Chaikin, Richard A. Register, and Douglas H. Adamson, Science **276** (5317), 1401 (1997); G. Krausch and R. Magerle, Adv Mater **14** (21), 1579 (2002); Wing Yan Chan, Alison Y. Cheng, Scott B. Clendenning, and Ian Manners, Macromolecular Symposia **209** (1), 163 (2004).

[9] Kyusoon Shin, K. Amanda Leach, James T. Goldbach, Dong Ha Kim, Jae Young Jho, Mark Tuominen, Craig J. Hawker, and Thomas P. Russell, Nano Lett **2** (9), 933 (2002); T. Thurn-Albrecht, R. Steiner, J. DeRouchey, C. M. Stafford, E. Huang, M. Bal, M. Tuominen, C. J. Hawker, and T. P. Russell, Adv Mater **12** (11), 787 (2000); S. Park, J. Y. Wang, B. Kim, J. Xu, and T. P. Russell, ACS Nano **2** (4), 766 (2008); Soojin Park, Jia-Yu Wang, Bokyung Kim, and Thomas P. Russell, Nano Lett **8** (6), 1667 (2008).

[10] P. L. Drzal, A. F. Halasa, and P. Kofinas, Polymer **41** (12), 4671 (2000); A. Sidorenko, I. Tokarev, S. Minko, and M. Stamm, Journal of the American Chemical Society **125** (40), 12211 (2003); William A. Phillip, Brandon O'Neill, Marc Rodwogin, Marc A. Hillmyer, and E. L. Cussler, Acs Appl Mater Inter **2** (3), 847 (2010).

[11] Rui Guo, Eunhye Kim, Jinsam Gong, Seunghoon Choi, Sujin Ham, and Du Yeol Ryu, Soft Matter **7** (15), 6920 (2011).

[12] K. A. Cavicchi and T. P. Russell, Macromolecules **40** (4), 1181 (2007).

[13] S. H Kim, M. J Misner, T. Xu, M. Kimura, and T. P Russell, Adv Mater **16** (3), 226 (2004).

[14] P. Mansky, J. DeRouchey, T. P. Russell, J. Mays, M. Pitsikalis, T. Morkved, and H. Jaeger, Macromolecules **31** (13), 4399 (1998).

[15] D. E Angelescu, J. H Waller, D. H Adamson, P. Deshpande, S. Y Chou, R. A Register, and P. M Chaikin, Adv Mater **16** (19), 1736 (2004).

[16] Hao Chen and Amitabha Chakrabarti, The Journal of Chemical Physics **108** (16), 6897 (1998).
[17] G. J. Kellogg, D. G. Walton, A. M. Mayes, P. Lambooy, T. P. Russell, P. D. Gallagher, and S. K. Satija, Phys. Rev. Lett. **76** (14), 2503 (1996).
[18] D. Y. Kwok and A. W. Neumann, Colloids Surfaces A: Physicochem. Eng. Aspects **161** (1), 31 (1999).
[19] Y. Wang, M. Rafailovich, J. Sokolov, D. Gersappe, T. Araki, Y. Zou, A. D. L. Kilcoyne, H. Ade, G. Marom, and A. Lustiger, Phys. Rev. Lett. **96**, 028303 (2006).
[20] O. H. Seeck, I. D. Kaendler, M. Tolan, K. Shin, M. H. Rafailovich, J. Sokolov, and R. Kolb, Appl Phys Lett **76** (19), 2713 (2000); T. Koga, Y. S. Seo, J. Jerome, S. Ge, M. H. Rafailovich, J. C. Sokolov, B. Chu, O. H. Seeck, M. Tolan, and R. Kolb, Appl. Phys. Lett. **83**, 4309 (2003).
[21] Simone Napolitano, Cinzia Rotella, and Michael Wübbenhorst, ACS Macro Letters **1** (10), 1189 (2012); C. Rotella, S. Napolitano, S. Vandendriessche, V. K. Valev, T. Verbiest, M. Larkowska, S. Kucharski, and M. Wubbenhorst, Langmuir **27** (22), 13533 (2011).
[22] Christian Ligoure and Ludwik Leibler, J. Phys. France **51** (12), 1313 (1990).
[23] Naisheng Jiang, Jun Shang, Xiaoyu Di, Maya K. Endoh, and Tadanori Koga, Macromolecules **47** (8), 2682 (2014).
[24] P. F. Green and T. P. Russell, Macromolecules **25** (2), 783 (1992).
[25] P. Mansky, T. P. Russell, C. J. Hawker, J. Mays, D. C. Cook, and S. K. Satija, Phys Rev Lett **79** (2), 237 (1997); E Huang, L Rockford, TP Russell, and CJ Hawker, Nature **395** (6704), 757 (1998); E. Huang, S. Pruzinsky, T. P. Russell, J. Mays, and C. J. Hawker, Macromolecules **32** (16), 5299 (1999).
[26] LarisaA Tsarkova, in *Nanostructured Soft Matter*, edited by AndreiV Zvelindovsky (Springer Netherlands, 2007), pp. 231.
[27] Sujin Ham, Changhak Shin, Eunhye Kim, Du Yeol Ryu, Unyong Jeong, Thomas P. Russell, and Craig J. Hawker, Macromolecules **41** (17), 6431 (2008).
[28] T. P. Russell, A. M. Mayes, V. R. Deline, and T. C. Chung, Macromolecules **25** (21), 5783 (1992).